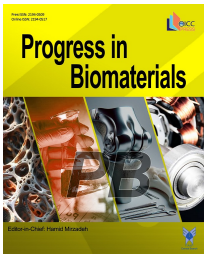

Volume 13, Issue 3, 132409 (1-15)

Progress in Biomaterials (PIBM)

https://doi.org/10.57647/pibm.2024.132409

Development and Evaluation of Biocompatible Scaffolds for Chronic Wound Healing and Biomaterials: Incorporating Vancomycin and Graphene Oxide

Alireza Jangi[1], Azadeh Asefnejad[1,*], Shahrokh Shojaei[2], Hessam Rezaei[1], Mohammad Mohammadi[1], Sara Gholizadeh[3], Foad Iranmanesh[4]

[1]*Department of Biomedical Engineering, SR.C., Islamic Azad University, Tehran, Iran.*
[2]*Department of Biomedical Engineering, CT.C., Islamic Azad University, Tehran, Iran.*
[3]*Department of Aesthetic and Restorative Dentistry, Faculty of Dentistry, Isf.C, Islamic Azad University, Isfahan, Iran.*
[4]*Department of Endodontic, School of Dentistry, Rafsanjan University of Medical Sciences, Rafsanjan, Iran.*

[*]**Corresponding author:** asefnejad_azadeh@iau.ac.ir

Original Research

Abstract:

Chronic wounds represent a considerable challenge for healthcare systems, necessitating the identification of effective wound dressings to facilitate healing. This study aimed to develop scaffolds utilizing biocompatible materials such as albumin and gelatin, with the incorporation of vancomycin for its antibacterial properties and graphene oxide nanoparticles to enhance mechanical strength. The scaffolds were fabricated through a freeze-drying technique and subsequently evaluated for morphology using scanning electron microscopy (SEM), functional groups via Fourier-transform infrared spectroscopy (FTIR), and assessed for swelling, biodegradability, along with various mechanical, biological, and antibacterial properties. The release profile of vancomycin from the G.5%Al.3%Go scaffold exhibited a more controlled pattern compared to that of the G.5%Al.1%Go scaffold. Additionally, immersion of the scaffolds in phosphate-buffered saline for 30 minutes indicated that increased graphene oxide content correlated with reduced swelling. Over a 15-day period, the degradation rate of the scaffolds revealed that the G.10%Al.3%Go scaffold degraded by up to 35%, while the G.5%Al.1%Go scaffold showed the lowest degradation rate at 18%. These results shows that the G.10%Al.3%Go scaffold may serve as a promising candidate for atopic treatment.

Keywords:

Albumin; Graphene oxide; Biomaterials; Vancomycin; Freeze-drying; Chemical stability

Cite this article: Jangi, A., Asefnejad, A., Shojaei, S., Rezaei, H., Mohammadi, M., Gholizadeh, S., Iranmanesh, F. Development and Evaluation of Biocompatible Scaffolds for Chronic Wound Healing and Biomaterials: Incorporating Vancomycin and Graphene Oxide. *Progress in Biomaterials* **13**(3), Article 09 (2024).

1. Introduction

Atopic dermatitis (AD), commonly referred to as atopic eczema, is a chronic inflammatory skin condition that affects millions, particularly infants and young children. This disorder is characterized by itchy, erythematous, and scaly skin lesions primarily located on the flexural surfaces of the body (Michailidou and Bikiaris, 2022; Berke et al., 2012; Azimi et al., 2017). The condition is attributed to a genetic deficiency in the protein filaggrin, which increases skin permeability, leading to heightened itching, scratching, and inflammation. The primary objective of managing AD is to minimize exacerbations and alleviate skin scaling (Hu et al., 2023; Wang et al., 2023a). Topical corticosteroids, delivered via ointments and lotions, are frequently employed to treat AD, aiming to enhance skin moisture and guard against corticosteroid-induced bacterial infections. Mast cells are implicated in the pathogenesis of AD; over 90% of AD patients exhibit colonization by *Staphylococcus aureus* in affected skin areas. Supernatants from *S. aureus* cultures exhibit significant mast cell granulation activity, with δ-toxin identified as a key granulation-inducing factor (Guo et al., 2022; Wang et al., 2023b; Alizadeh et al., 2013). The colonization of skin by *Staphylococcus aureus* triggers the production of interleukin IL-4, contributing to allergic skin diseases. Additionally, vancomycin has been shown to induce mast cell degranulation. Gelatin, derived from collagen, is recognized as a promising candidate for skin

tissue engineering and repair due to its high biocompatibility, biodegradability, and safety profile (Nasalapure et al., 2017; Ng et al., 2015; Grajales et al., 2023). Furthermore, gelatin possesses properties such as adhesion, water retention, and the ability to activate platelets, thereby enhancing hemostasis. In contrast to other biological materials that necessitate complex purification, manufacturing processes, or incur high costs, egg white is an easily accessible and economical protein. An egg white has historically been used as a poultice for burn treatment and wound healing. Albumin, the most abundant protein in egg white, enhances cell adhesion and proliferation. Lysozyme exhibits intrinsic antibacterial properties against both Gram-positive and Gram-negative bacteria by cleaving the β-1,4 bond in the bacterial cell wall in both its native and denatured forms (Carr, 2013; Hu et al., 2009; Yang et al., 2012; Homem et al., 2022). In comparison to traditional materials like collagen, egg white demonstrates superior absorption of cytokines and promotes neoangiogenesis (Kumar et al., 2013; Andrijanto et al., 2016; Derkach et al., 2019). However, much of the existing research has focused on egg white as a source of bioactive compounds rather than as a hydrogel material. Graphene oxide possesses a large surface area and numerous functional groups; even a small quantity can enhance the mechanical properties, electrical conductivity, biocompatibility, and antibacterial activity of scaffolds. High concentrations of graphene oxide can induce cytotoxicity and diminish biocompatibility (Kalil et al., 2018; Michailidou and Bikiaris, 2022; Zhao et al., 2012; Hoseini-Ghahfarokhi et al., 2020; Abdelhamid and Hussein, 2021). Therefore, determining the optimal concentration of graphene oxide is essential for effectively modifying scaffolds to promote skin wound healing (Huang et al., 2012; Piao and Chen, 2016; Shuai et al., 2018). The freeze-drying process, based on the principle of sublimation, is utilized to prepare porous scaffolds. In this method, a polymer is dissolved in an appropriate solvent, and water is added to create an emulsion (Alili-Firoozinezhad et al., 2015; Dong and Zhang, 2020; Farrar et al., 2010). The emulsion is then poured into a mold, frozen using liquid nitrogen, and subsequently dried to eliminate the solvent and frozen water. This technique avoids the use of high temperatures and eliminates the need for a separate leaching step; however, it typically results in a low pore size and involves a lengthy processing time (Kumar et al., 2014; Sangeetha et al., 2018).

This research shows the design and fabrication of 3D scaffolds utilizing biopolymers through the freeze-drying technique, specifically focusing on a formulation comprising gelatin, albumin, graphene oxide, and vancomycin. Various scaffold compositions were developed, and their physical and morphological characteristics were evaluated using techniques such as field emission scanning electron microscopy (FESEM) and Fourier-transform infrared spectroscopy (FTIR). The optimal scaffold was selected for further biological assessments, including cell culture and MTT assays. Given the significant damage statistics related to this vital soft tissue, there is a pressing need for alternatives that possess biomimetic properties. In this study shows the integration of natural materials like gelatin and albumin as foundational components for tissue repair. Graphene oxide was incorporated to enhance mechanical properties, while vancomycin was utilized for its antibacterial effects, alongside natural polymers to improve skin hydration. The freeze-drying technique was chosen for its capacity to produce suitable scaffold designs.

2. Materials and methods

2.1 Required materials and equipment

Table 1 is related to the materials used in the project. Also, the devices and equipment used in the studies are listed in Table 2.

Table 1. Specifications of materials used in making samples and tests.

Description	Company	Material name
Mw = 477.550 g/mol $C_{31}H_{27}NO_4$ ...	Sigma-Aldrich	Gelatin
Molecular Weight: ...g/mol	Sigma-Aldrich	Graphene oxide
		Vancomycin
CH_3COOH Molecular Weight: 60.052 g/mol	Sigma-Aldrich	Acetic acid
PH = 7.3 ± (0.1)	DNAbiotech	Phosphate-buffered saline solution
H_2O Molecular Weight: 18.01528 g/mol	Zalal-Iran	deionized water
$CaCl_2 \cdot 2H_2O$ Molecular Weight: 110.98 g/mol	Gatran Shimi-Iran	Calcium chloride
HCl Molecular Weight: 36.46 g/mol	Neutron-Iran	Hydrochloric acid

Table 2. Equipment and devices used in the experiments.

Device brand	Device model	Equipment name
Japan, FX300I	AND	Digital scale
China, Alfa	H5-860	Stirrer/Hot Plate
China	Va-5II	Drying-freezing
BOMEM	SRG 1100G	Infrared spectroscopy
Serontechnologies	AIS2100	SEM
Bell/Italy	MP-bell	Optical microscope
Sarv Tehiz - Iran	—	Laboratory hood
Germany - Philips	PW1730	X-ray spectroscopy (XRD)
Iran	—	Falcon
Branches	HB170	Centrifuge

2.2 Preparation of samples

2.2.1 Albumin extraction polymer

Initially, the whites of 5 eggs were thoroughly combined, using 3 cc of saline solution for every 1 cc of egg white. The saline solution was prepared by dissolving 9 g of sodium chloride and 4 mM of EDTA in 1 liter of distilled water. The resulting mixture of egg white and saline was placed on a magnetic stirrer and stirred for 1 hour at room temperature. The pH of the mixture was adjusted to 4.5 by adding half-normal hydrochloric acid, after which the solution was stirred for an additional 30 minutes. The prepared solution was then transferred to a Falcon tube and centrifuged for 10 minutes. The sediment formed at the bottom of the Falcon tube was discarded, while the supernatant was retained for subsequent analyses.

2.2.2 Fabrication of three-dimensional scaffold

Initially, 1.5 g of gelatin was dissolved in 50 mL of distilled water. In containers labeled A and B, extracted albumin was added to achieve a concentration of 5 wt.%. These mixtures were then placed on a magnetic stirrer at a rotation speed of 600 rpm for 4 hours at ambient temperature to ensure complete homogeneity. Subsequently, 1% by weight of graphene oxide was incorporated into glass A, while 3 wt.% was added to glass B. In containers C and D, a 10% by weight concentration of albumin was utilized, and after ensuring complete dispersion of graphene oxide, 1% and 3% by weight were added, respectively. A consistent proportion of 2% by weight of vancomycin was included in all solutions. 0.5 cc of glutaraldehyde was added as a crosslinking agent to each milliliter of the solution. The prepared solutions were then transferred into specialized containers for freeze-drying.

Freeze-drying, or lyophilization, is a method that involves drying a product at low temperatures under vacuum conditions. In this process, the sample is first frozen, transforming the water into a solid state, and then the ice is sublimated directly into vapor without passing through a liquid phase. A key advantage of freeze-drying is that the samples remain at low temperatures throughout the drying process, preserving heat-sensitive components and maintaining the original shape and size of the material. Consequently, the dried products can be stored for extended periods without risk of compositional changes or microbial contamination, owing to the absence of water. The samples were initially placed in a freezer for 24 hours and then in a nitrogen environment until they were completely frozen, after which they were immediately transferred to the freeze dryer for a duration of 24 hours. Following the freeze-drying process, the samples were prepared for various analyses. Figure 1 (a) shows the equipment used, while figure 1 (b) illustrates the resulting scaffolds.

Figure 1 (a-b) shows a detailed overview of the study's key components. Figure 1 (A) shows features the freeze-drying machine used in the research. The freeze-drying process, or lyophilization, is crucial for preserving sensitive materials by removing moisture while maintaining structural integrity.

2.3 Materials characterization

2.3.1 Identification of operative groups

2.3.1.1. Fourier transform infrared spectroscopy (FTIR)

The spectrometer (FTIR) can measure the transmission spectrum and the absorption spectrum in the wavelength range of 400 cm^{-1} to 4000 cm^{-1}. The device can identify and analyze compounds that have infrared absorption bands. Using an infrared spectrometer SRG 1100G model, the experiment was performed for 3D scaffolds.

2.3.2 Morphological examination

2.3.2.1. Optical microscope

An optical microscope was used for the initial observation of the scaffolds and examination of the surface and porosity. The optical microscope used is the MP-Bell model, which was made for 3D scaffolds.

2.3.3 Scanning electron microscope (SEM)

A scanning electron microscope (SEM) was employed to investigate the surface characteristics and morphology of the scaffold. To enhance the conductivity of the samples, a gold coating was applied. The samples were placed in a vacuum chamber and subsequently coated with gold using gold particles in a plasma deposition process. The SEM utilized for this analysis was the AIS2100 model, specifically designed for examining electrospun scaffolds.

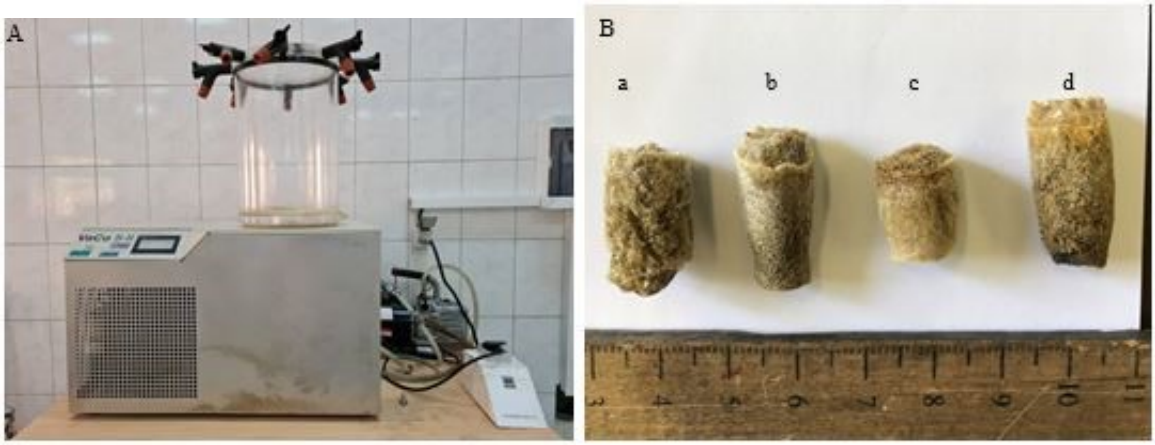

Figure 1. Image (A) A view of the freeze-drying machine, Image (B) Fabricated scaffolds, (a) G.5%Al.1%Go, (b) G.5%Al.3%Go, (c) G.10%Al.1%Go, and (d) G.10%Al.3%Go.

2.3.4 Scaffold inflation check

To evaluate the degree of swelling and water absorption, a swelling test was conducted. Initially, the samples were weighed to determine their dry weight. Following immersion in a phosphate-buffered saline (PBS) solution, the samples were weighed again to obtain their wet weight. The swelling rate over a 30-hour period was calculated using equation (1). Figure 2 (a-d) illustrates the samples submerged in the PBS solution.

$$\text{Inflation percentage} = \frac{W - W_0}{W_0} \times 100 \qquad (1)$$

where W_0 is the dry weight and W is the weight of the submerged scaffold.
Figure 2 shows the placement of the scaffold samples in PBS solution, including formulations (a) G.5%Al.1%Go, (b) G.5%Al.3%Go, (c) G.10%Al.1%Go, and (d) G.10%Al.3%Go, highlighting their respective swelling behaviors during the experiment.

2.3.5 Biodegradability

A biodegradability test was conducted to assess the stability and measure the degradation rate of the scaffold in an external environment. Initially, the scaffold was weighed to determine its dry weight and then immersed in PBS for 15 days. At 24-hour intervals, the samples were removed from the solution, dried using filter paper, and weighed. The percentage of scaffold biodegradability was calculated using equations (2) and 3.

$$\text{Biodegradability percentage} = \frac{W_0 - W}{W_0} \times 100 \qquad (2)$$

where W_0 is the dry weight and W is the weight of the submerged scaffold.

2.3.6 Checking mechanical properties

2.3.6.1. Compressive strength

In this test, the scaffold is positioned between 2 plates that distribute the applied force across opposing surfaces of the sample. These plates are subsequently pressed together using the Hi-500kg-SE universal testing device, resulting in the flattening of the sample, as illustrated in figure 3.
When subjected to compression, the sample typically shortens in the direction of the applied force while expanding in the perpendicular direction. The objective of pressure testing is to assess the material's behavior or response by measuring variables such as strain, stress, and deformation under applied compressive forces. Pressure tests were conducted on the three-dimensional coated scaffolds using the ZEMIC load cell model H3-C3-50kg-3B-D55 (see figure 3).

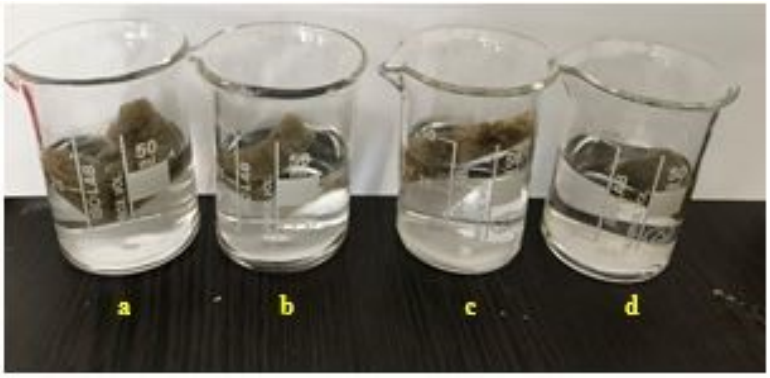

Figure 2. Placement of samples in PBS, (a) G.5%Al.1%Go, (b) G.5%Al.3%Go, (c) G.10%Al.1% Go, and (d) G.10% Al.3%Go.

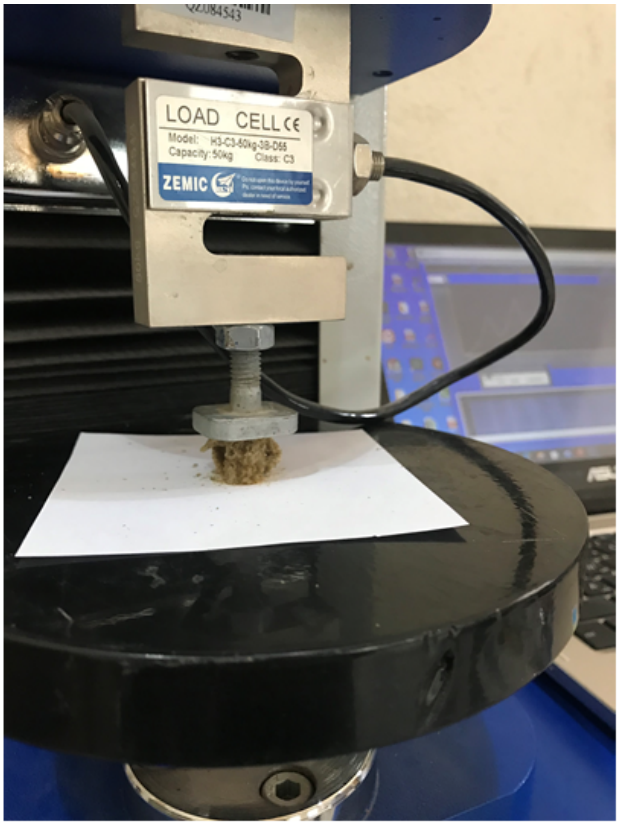

Figure 3. Device used for pressure test.

2.3.7 Drug release

2.3.7.1. Standard curve

The initial concentration of vancomycin was 2 ppm, which was subsequently diluted with PBS to prepare four different concentrations for the standard curve. The absorbance of these samples was measured using a UV spectrophotometer. The area under the peak was calculated for each concentration at a wavelength of 203 nm, allowing for the construction of a standard curve for vancomycin concentration based on UV absorption. Figure 4 illustrates the schematic of the antibacterial test process utilizing the disc diffusion method. This technique involves placing antibiotic-impregnated discs on an agar plate inoculated with bacteria. The resulting inhibition zones are measured to assess the antibacterial efficacy of the tested materials, providing critical insights into their potential therapeutic applications.

The equation of the line for the vancomycin standard graph was determined to be $R^2 = 0.7778$, with the relationship described by the equation $x = 0.0003 - 0.0005\ x$.

2.3.7.2. Dialysis bag preparation

The quantity of vancomycin extract loaded into the scaffold and the amount of drug released were quantified using UV spectrometry. To prepare the dialysis bag for the release test, it was immersed in a solution containing 2% (w/v) baking soda and 0.05% (w/v) EDTA for 30 minutes. Following this, the bag was rinsed with double-distilled water and subsequently placed in boiling double-distilled water.

2.3.7.3. Checking the amount of drug release

To conduct the tests, one end of the dialysis bag was secured before inserting the sample. This end was then tied with thread or clipped at the double-layered section to prevent damage to the bag. 4 mg of the drug-containing scaffold was placed into the dialysis bag, which was then sealed at the other end. A total of 30 mL of PBS solution was added to a container, and the dialysis bag containing the samples was immersed to ensure that its entire surface was submerged. The container was then covered and placed in a water bath maintained at 37 °C, with the samples agitated on a shaker. During the first two hours, samples were taken every 30 minutes, followed by hourly sampling for the subsequent 8 hours. During each sampling interval, 4 mL of PBS solution surrounding the dialysis bag was removed and replaced with an equal volume of fresh PBS solution. It is important to note that the container lid remained closed throughout the sampling periods. The collected samples were analyzed using a UV spectrophotometer, and the percentage of drug release was calculated to determine the amount of vancomycin released from the scaffold over time.

2.3.8 Identification of elements and microstructure

2.3.8.1. X-ray differential diffraction analysis (XRD)

To study the crystal structure and check the phase composition of the samples, an X-ray differential diffraction analysis was performed. The phase composition was evaluated by X-ray diffraction (XRD) (PW1730-Philips) by scanning in the Bragg-Brentano geometry using radiation ($k = 1.5406$ Å). The experimental conditions used were 1.5 hours of scanning time with 2 hours of 0.020° scanning stage and a scanning range between 4° and 90°, with a measurement time of 50 seconds in each stage. The parameters of the X-ray generator are voltage 45 kV and intensity 40 mA. The anode is copper and the filter is nickel. The stopping time in each step is one second, the step size is 0.02 degrees, and the patterns are identified using references. X-ray diffraction analysis was performed for 3D scaffolds.

2.3.8.2. Elemental identification analysis (Eds)

The Energy Dispersive Spectroscopy (EDS) analysis, utilizing the AIS2100 model specifically designed for three-dimensional scaffolds, enables the semi-quantitative identification of the constituent elements of the sample, requiring a minimum of 5 mg of the particle sample. This analysis can identify elements ranging from carbon to uranium, providing both point and semi-quantitative assessments. Additionally, the EDS test presents the energy spectrum of the sample and is capable of detecting concentrations from 0.1% to 100%.

2.3.9 Cell culture test (*in vitro*)

2.3.9.1. Culture of fibroblast cells

The cell culture test was conducted by the ISO10993-5 standard and indirectly. To prepare one-day extracts, first, one sample with dimensions of 3 square centimeters was prepared and placed inside a sterile microtube. Then one milliliter of RPMI culture medium without FBS was poured on them and placed inside the incubator. The cultivation conditions inside the incubator include 5% CO_2 carbon dioxide gas, 90% humidity, and 37 °C cultivation temperature. The floor of the 12-house plate was also used as a negative control to detect the lack of cytotoxicity response. Dimethyl

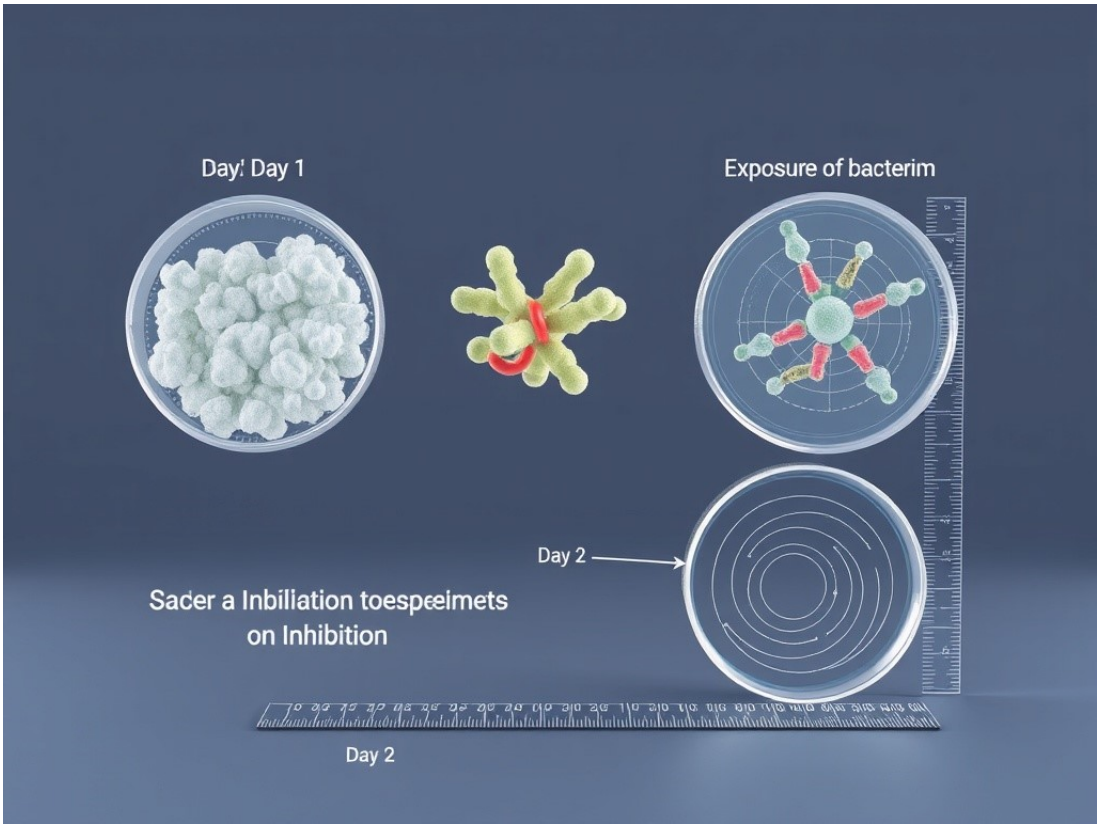

Figure 4. Schematic of antibacterial test process using disc diffusion method.

thiazyl diphenyl tetrazolium bromide (MTT) test with a concentration of 0.5 mg/mL was used to evaluate toxicity. Thus, first, 5000 L929 cells in 100 microliters of culture medium (RPMI) containing serum were poured into three wells of a 12-well plate for each of the two samples and one column as a control. After one day, the culture medium was removed 100 microliters of extract containing 10% serum was added to each well and FBS-containing medium was added to the control column. After 24 hours, the extract was removed and 100 microliters of MTT solution was poured into each well. After four hours, the medium on the cells was removed and 100 microliters of isopropanol was added to them and placed in the incubator for 20 minutes to dissolve the purple formazan crystals. Then, the absorbance of the substance dissolved in isopropanol was calculated at a wavelength of 545 nm with an ELISA reader (Stat Fax 2000). The well with more cells shows a higher optical density (OD) than the well with fewer cells. Therefore, it can be determined from the relationship below the well with more cells and compared with the control sample.

$$\text{Toxicity}\% = \left(1 - \frac{\text{mean OD of sample}}{\text{mean OD of control}}\right)$$

$$\text{Viability}\% = 100 - \text{Toxicity}\%$$

In living cells, the color of MTT in the mitochondria transitions from yellow to purple formazan crystals, with the intensity of the color serving as an indicator of cell viability. The percentage of cell survival is represented by the data presented in the graphs of the following chapter, which demonstrate the non-toxicity of the samples.

2.3.9.2. Proliferation of fibroblast cells

In this research, an L929 cell (NCBI C161) obtained from the cell bank of the Pasteur Institute of Iran was used. After freezing the cells, they were transferred to a flask containing DMEM culture medium with 10% FBS and then the flask was placed in an incubator at 37 °C, 90% humidity, and 5% carbon dioxide concentration. It should be noted that the culture medium was changed every 3-4 days.

2.3.9.3. Sample preparation

First, the sample was cut in dimensions of 1 × 1 cm and placed in the bottom of the wells of the culture plate of 12 houses. Next, the samples were first sterilized with 70% alcohol and then with UV.

2.3.9.4. Cell adhesion test

To assess cell adhesion, sterilized samples were placed in each well of a sterile 12-well plate. Subsequently, 20,000 cells in a volume of 80 microliters were added to each sample and incubated for 4 to 5 hours to allow for cell adhesion. Following this incubation period, a specified volume of culture medium containing 10% fetal bovine serum (FBS) was added to each well. After 24 hours, the culture medium was removed, and the samples were washed with PBS for 30 seconds. Then, 3.5% glutaraldehyde was applied for cell fixation. After applying the fixative to each sample, they were stored in a refrigerator for 2 hours. The fixative was then removed, and the samples were rinsed with deionized water, followed by washes with alcohols at concentrations of 50%, 60%, 70%, 80%, and 96%. Finally, cell adhesion to the samples was examined using an AIS2100 SEM.

2.3.10 Antibacterial reaction

One method for assessing the antibacterial properties of a substance involves measuring the diameter of the inhibition zone. In this technique, a specific number of isolated bacteria is suspended in serum medium and cultivated as a lawn on Mueller Hinton Agar plates. The tested samples are then placed onto the culture medium. After incubating the plates at 37 °C for 24 hours, they are examined under light to measure the area of inhibition. In the disc diffusion method, the agar plate is inoculated with a standardized amount of the test microorganism, followed by the placement of a disc (approximately 6 mm in diameter) containing the test compound at the desired concentration on the agar surface. The Petri dish is then incubated under appropriate conditions. Typically, the antimicrobial agent diffuses through the agar, inhibiting the growth of the microorganism, after which the diameter of the inhibition zone is measured. Antibiograms classify bacteria into sensitive, semi-sensitive, or resistant categories based on qualitative results, making this method essential for determining resistance phenotypes among tested bacteria. These results can provide valuable insights for experts. Escherichia coli and Staphylococcus bacteria are evenly spread onto Petri dishes containing solid LB medium, following the McFarland standard for concentration.

3. Results and disscusion

Many studies introduced an injectable polyzwitterionic lubricant aimed at stopping cardiac adhesions, while another explored lecithin-based electrospun nanofibers to reduce abdominal adhesions. These advancements hold promise for improving patient outcomes in surgical care (Wang et al., 2023c; Mirhaj et al., 2022; Zhou et al., 2022; Tavakoli et al., 2022). Recent research in composite and biomaterials has revealed exciting developments. One study investigated reinforced composite structures in acidic environments, while another examined the mechanical behavior of glass fiber reinforced polymer (GFRP) composites under similar conditions (Rahmani et al., 2023b; Dadras et al., 2023; Gitiara et al., 2021; Barbaz-Isfahani et al., 2023b). Additionally, the impact of nanoclay and nanosilica on GFRP composites in corrosive settings was analyzed. The synergistic effects of eggshell powder and halloysite clay nanotubes on the properties of polypropylene composites were also explored (Rahmani et al., 2023a; Kamarian et al., 2023; Barbaz-Isfahani et al., 2023a; Alimirzaei et al., 2024; Barbaz-Isfahani et al., 2022; Barbaz-Isfahani et al., 2023c). Recent developments in composite materials, nanoparticles, and biomaterials have revealed promising applications across various fields (Farazin et al., 2021; Liang et al., 2022; Moarrefzadeh et al., 2023; Safaei et al., 2023; Khandan et al., 2020; Jaberi et al., 2022). One study focused on creating a 3D bioprinted alginate-gelatin hydrogel scaffold enriched with calcium phosphates for dental pulp regeneration (Attaeyan et al., 2024; Qian et al., 2020; Rajaei et al., 2022; Asefnejad, 2024). Other research aimed to improve the characteristics of polyvinyl alcohol/chitosan matrices by incorporating magnesium and silicon modifications (Oudeh Kadhim et al., 2024; Ghomi et al., 2024; Dehkordi et al., 2023; Javidan Bashiz et al., 2024). Additionally, studies examined the mechanical properties of titanium-reinforced ceramics and the use of nanoparticles in scaffolds for bone tissue engineering (Raisi et al., 2020; Jasemi et al., 2022; Moghadas et al., 2024; Sheikhbahei and Ari, 2024; Ghafari et al., 2024). These advancements seek to enhance therapeutic outcomes and improve material performance in medical and industrial contexts (Shahmirzadi et al., 2024; Tavakoli et al., 2024; Zakavi et al., 2023; Bahari et al., 2021; Bahari et al., 2019). Figure 5 shows light microscope images of the three-dimensional porous scaffolds. The images indicate that the G.5%Al.1%Go and G.10%Al.1%Go scaffolds show irregular porosities. In contrast, the porosity of the G.5%Al.3%Go and G.10%Al.3%Go scaffolds appears more uniform and parallel. A FE-SEM was utilized. Recent research has made exciting progress in preventing postoperative adhesions and immune responses through innovative materials.

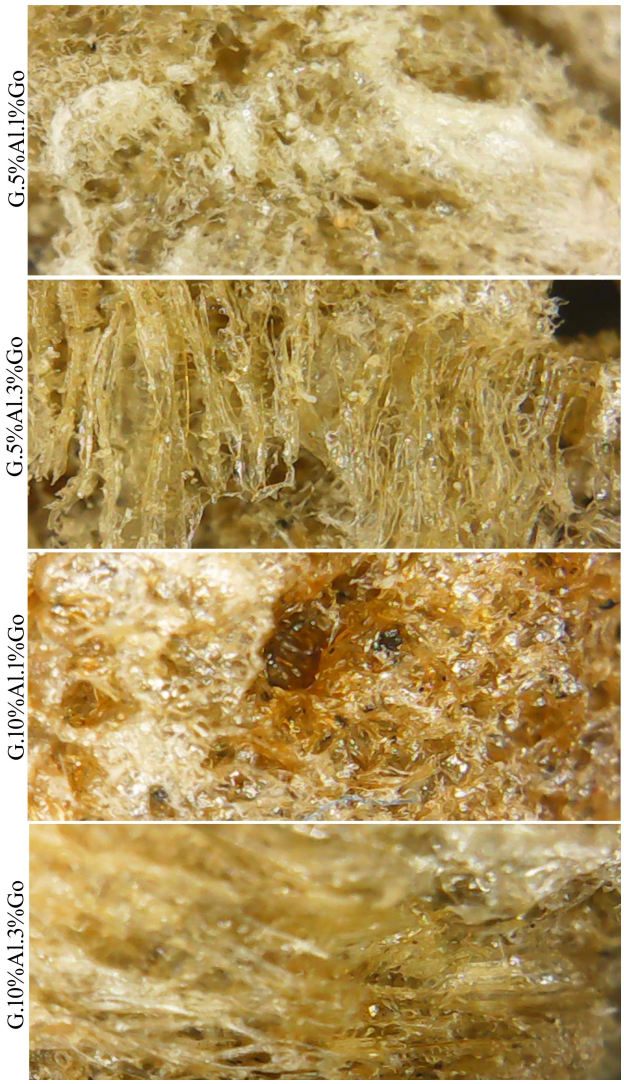

Figure 5. Optical microscope of (a) G.5%Al.1%Go, (b) G.10%Al.1%Go, (c) G.5%Al.3%Go, and (d) G.10%Al.3%Go scaffolds.

The morphology of the porous three-dimensional scaffolds was analyzed using a SEM, as illustrated in figure 6 (a-d). SEM images correspond to the G.5%Al.1%Go and G.10%Al.1%Go scaffolds, with pore sizes ranging from 209 to 50 micrometers and 515 to 50 micrometers, respectively.

The layers formed in these two scaffolds exhibit irregular porosity. The porous structure of the scaffolds containing 1% Go did not show distinctive characteristics in terms of channel formation, as previously noted, instead developing a spherical porous structure with a three-dimensional arrangement and interconnections, as depicted in figure 6 (a-d).

Figure 7 (a-d) illustrates that the formation of parallel plates occurs with an increase in the weight percentage of Go. A comparable channel structure was observed in the freeze-dried hydrogel produced by lyophilization. In this instance, however, the plates were interconnected by thin bridges, as showed in figures 7 (b-d).

Research has showed that graphene possesses exceptionally high thermal conductivity, making it valuable in the electrical industry for enhancing the thermal conductivity of polymers, such as plastics and silicone gels. In contrast, graphene oxide exhibits lower thermal conductivity due to the transition of hybridized carbon atoms from sp^3 to s^2 configuration. This alteration affects phonon transfer within sp^2 domains, resulting in the formation of low-resistance channels. When ice crystals experience external stress, such as rapid cooling, their orientation is influenced by the temperature gradient created by the gelatin hydrogel. The authors observed that temperature variations lead to the development of thin connections between the plates, likely resulting in a lower temperature environment that facilitates the alignment of ice crystals and minimizes random crystallization.

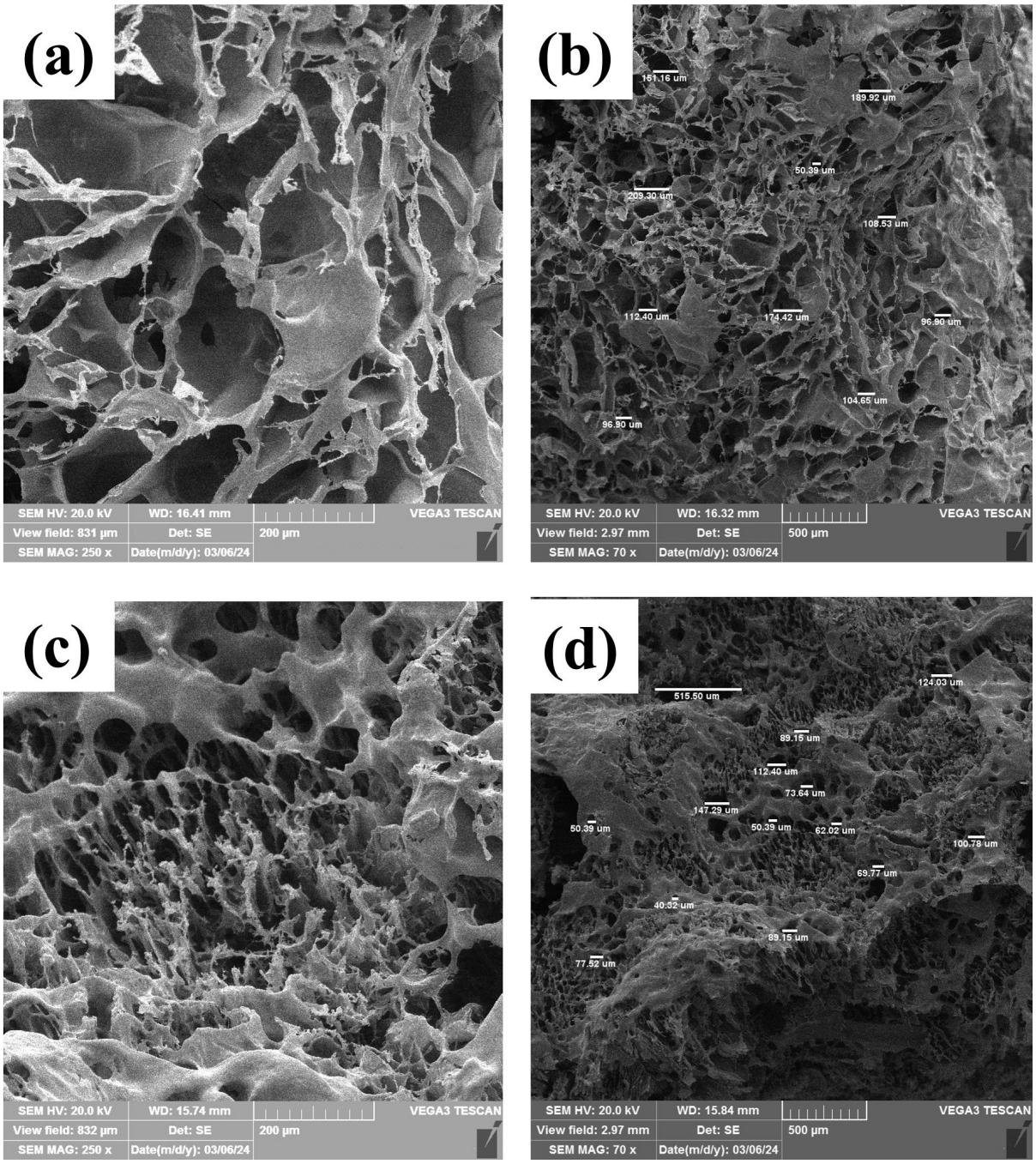

Figure 6. SEM image, (a-b) G.5%Al.1%Go, (c-d) G.10%Al.1%Go.

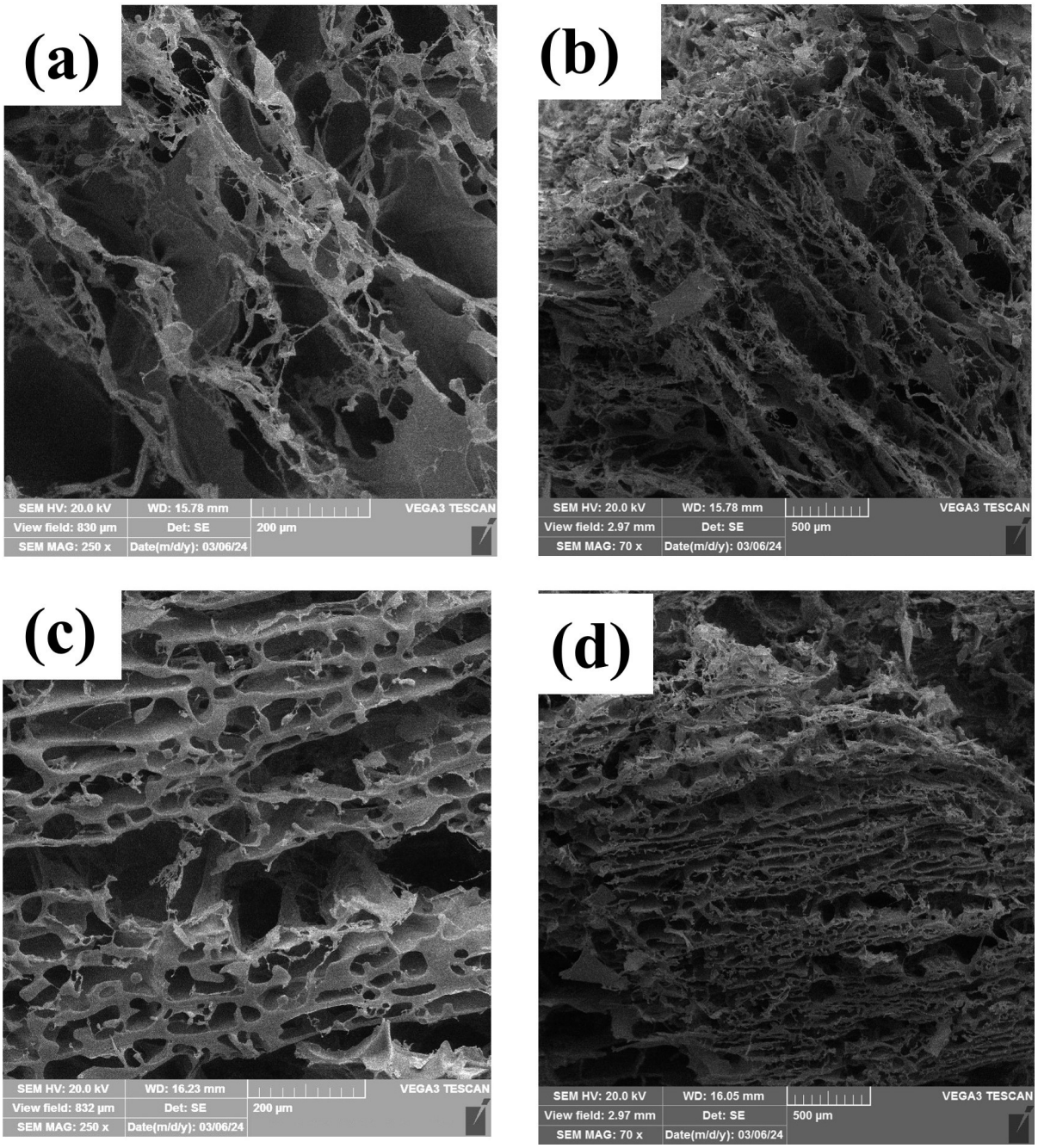

Figure 7. SEM image, (a-b) G.5%Al.3%Go, (c-d) G.10%Al.3%Go.

3.1 Identification of operative groups

3.1.1 Infrared spectroscopy (FTIR)

Figure 8 shows the peaks associated with graphene oxide (GO) as observed in the Fourier-transform infrared (FTIR) spectrum. The hydroxyl group (C-OH, phenol) appears within the range of 3050-3800 cm^{-1}, while the peak at 1070 cm^{-1} corresponds to the C-O vibrations of carboxylic acid (COOH) and water (H_2O). The peak observed at approximately 3418-3412 cm^{-1} is attributed to the O-H stretching vibrations of C-OH groups and the water content in the material. Various oxygen configurations related to the GO structure exhibit vibrations in the ranges of 1234-1236 cm^{-1} (C-O-C epoxide), 1533 cm^{-1} (C=C hybrid, in-plane vibrations), and 1642-1652 cm^{-1} (carboxyl COOH). An increasing the weight ratio of GO in the G.5%Al.3%Go scaffold has intensified the COOH peak. According to the research conducted by Andrijanto et al. (Andrijanto et al., 2016), a peak in the range of 1720 cm^{-1}, associated with the carbonyl stretching group (C=O), was not detected in this study due to the presence of other substances.

In the FTIR spectrum, the presence of albumin was indicated by peaks at 1652-1642 cm^{-1} corresponding to the C=O stretching of the amide I band, and at 1533 cm^{-1} related to C-N stretching with bending mode (N-H), indicative of the amide II band, confirming the presence of protein in albumin. Additionally, peaks associated with gelatin are observed in the range of 1389 cm^{-1}, corresponding to the amide III band. Research conducted by Svetlana R. Derkach

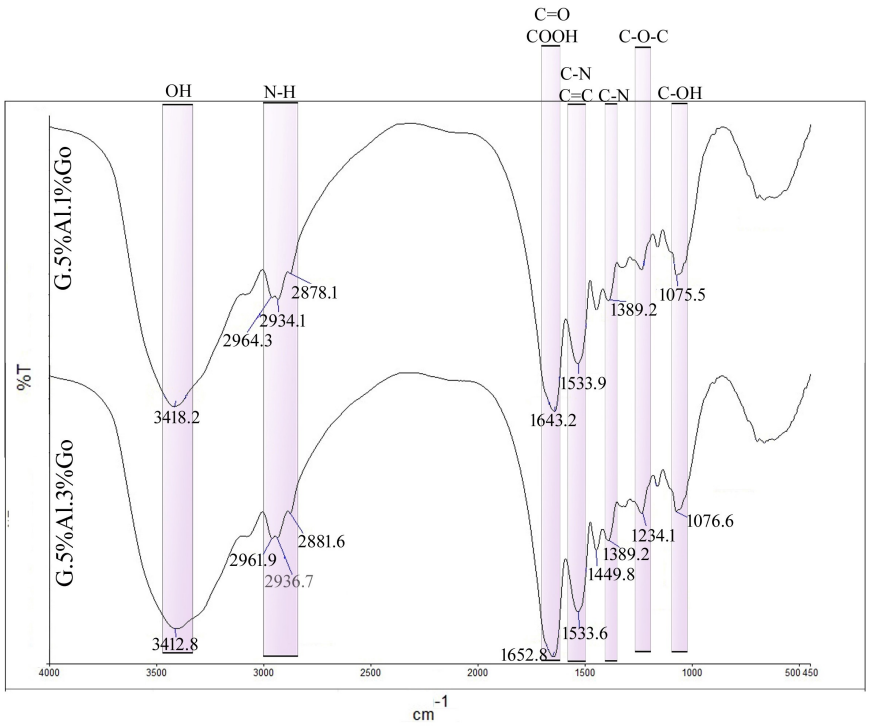

Figure 8. Infrared spectroscopy, G.5%Al.1%Go and G.5%Al.3%Go scaffolds.

and colleagues (Derkach et al., 2019) has demonstrated that gelatin's chemical structure includes amides A and B, as well as amides I, II, and III. It is important to note that the detection of these groups can vary depending on the type of gelatin used. The peak in the range of 2951-2878 cm^{-1} corresponds to the N-H stretching vibration of amide B. Figure 9 illustrates the FTIR spectrum for the G.10%Al.1%Go and G.10%Al.3%Go scaffolds, clearly showing all identified peaks related to graphene oxide, albumin, and gelatin. Figure 10 illustrates the process of synthesizing graphene oxide from graphite. The schematic shows the presence of carboxyl (COOH) and hydroxyl (OH) functional groups, which were identified in the FTIR peaks.

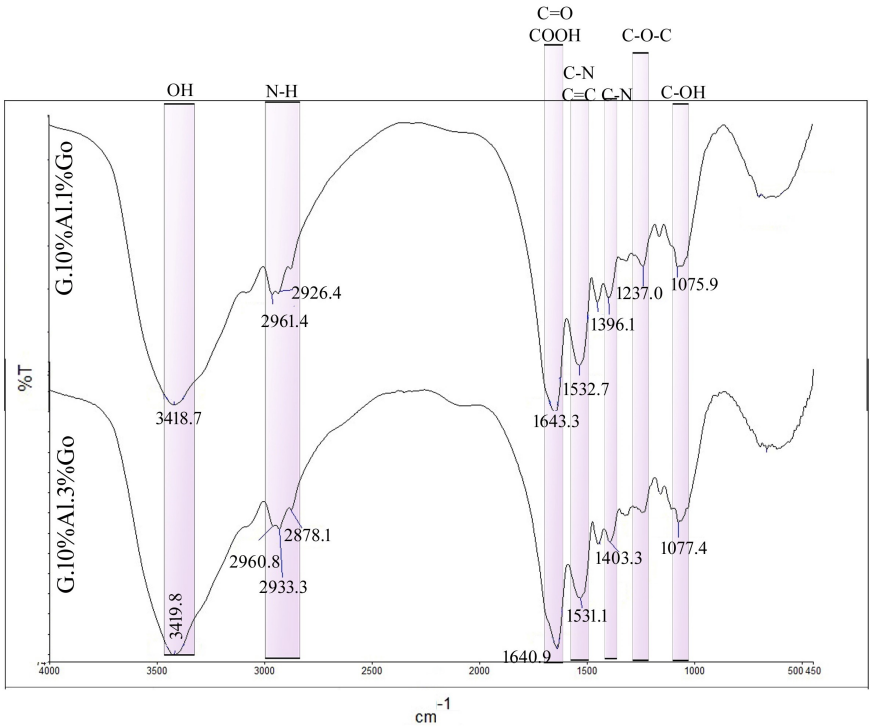

Figure 9. Infrared spectroscopy, G.10%Al.1%Go and G.10%Al.3%Go scaffolds.

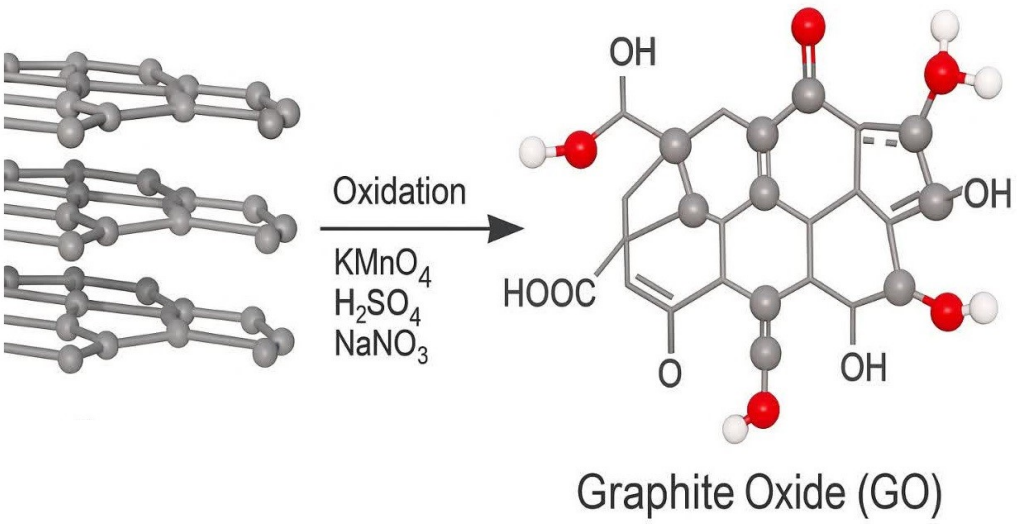

Figure 10. Graphene oxide production schematic.

3.2 Identification of elements using EDS test

The weight and atomic percentages of elements including carbon (C), oxygen (O), and nitrogen (N) were analyzed using X-ray energy dispersive spectroscopy. Figure 11 presents the weight and atomic ratios of these elements for each scaffold. The weight percentages of C and O for the G.5%Al.1%Go and G.5%Al.3%Go scaffolds were found to be 33% and 44% for carbon, and 25% and 52% for oxygen, respectively.

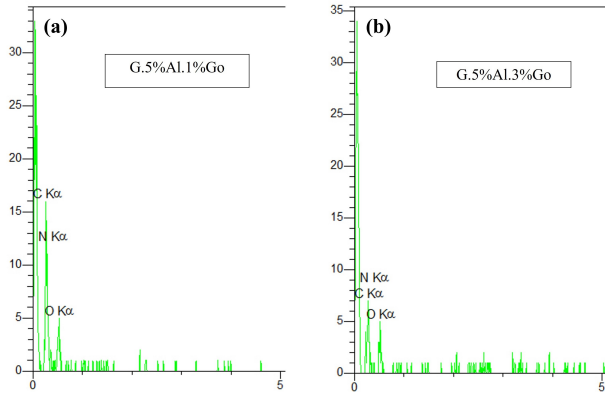

Figure 11. X-ray energy diffraction spectroscopy for (a) G.5%Al.1%Go and (b) G.5%Al.3%Go scaffolds.

The weight percentage of nitrogen (N) for both scaffolds is between 21% and 22%. The results indicate that the nitrogen weight percentage does not influence the increase of graphene oxide (GO). However, as the amount of GO rises, the weight percentage of carbon (C) decreases while that of oxygen (O) increases. Research has shown that the weight percentage of oxygen is greater than that of carbon. Figure 12 (a-b) shows the energy dispersive spectroscopy (EDS) spectrum for the G.10%Al.1%Go and G.10%Al.3%Go scaffolds, with the weight percentages of C and O being 40% for the G.10%Al.1%Go scaffold and 36% and 45% for the G.10%Al.3%Go scaffold, respectively. In contrast, the weight percentage of nitrogen for scaffolds containing 5% albumin remains within the range of 21% to 22%.

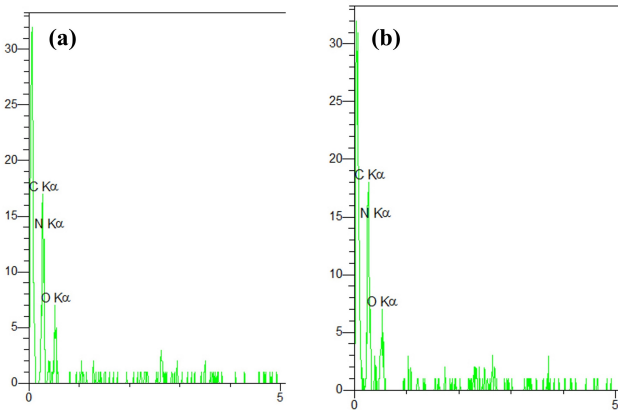

Figure 12. X-ray energy diffraction spectroscopy for (a) G.10%Al.1%Go and (b) G.10%Al.3%Go scaffolds.

3.3 Drug release

The primary objective of designing an optimal drug delivery system is to administer therapeutic agents within the patient's body in a controlled manner while minimizing side effects on healthy tissues. Due to the limited solubility of certain chemotherapy drugs in water and their lack of specificity in targeting affected tissues, these drugs frequently result in significant adverse effects on non-target tissues. In recent decades, advancements in tissue engineering have addressed some of these challenges by introducing nano-sized drug carriers that are effective in drug release systems. Nanomedicine has expanded its applications to include bacterial inhibitors, imaging contrast agents, and drug/gene delivery systems, owing to its favorable properties, biocompatibility, and operational ease. Graphene nanostructures present a promising option as drug-loading agents. Figure 13 shows the drug release process over a period of 25 hours. The data indicate that the G.5%Al.3%Go scaffold shows a higher release rate of approximately 28% within the first 5 hours, whereas the G.5%Al.1%Go scaffold

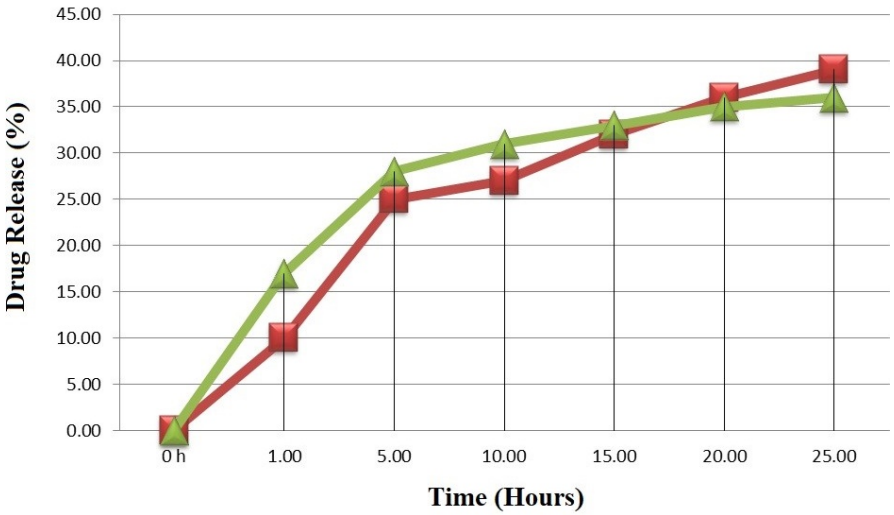

Figure 13. Drug release rate for 25 hours, G.5%Al.1%Go and G.5%Al.3%Go.

shows a release of about 24% during the same timeframe. After 25 hours, the drug release rate for the G.5%Al.3%Go scaffold (36%) was lower than that of the G.5%Al.1%Go scaffold (40%), indicating that the G.5%Al.3%Go scaffold exhibits controlled release characteristics. This phenomenon may be attributed to the increased proportion of graphene oxide. The drug is intercalated between the layers of graphene oxide, and as the weight ratio of graphene oxide rises, a greater quantity of drug is encapsulated within these layers.

4. Conclusion

Tissue engineering and the replacement of damaged tissues play a crucial role in medical science, often proving to be more effective than organ transplantation between individuals. The development of wound dressings from both natural and synthetic polymers with desirable properties for tissue regeneration is rapidly progressing. The materials used in scaffold fabrication can be natural, synthetic, or mineral-based, and they must exhibit biocompatibility and biodegradability. Additionally, hydrophilicity is an important characteristic for scaffolds. Natural polymers such as gelatin, chitosan, and alginate demonstrate good hydrophilicity and biocompatibility; however, they lack inherent antibacterial properties. This research aimed to prepare scaffolds utilizing biocompatible materials, specifically albumin and gelatin, while incorporating vancomycin to impart antibacterial properties. Moreover, graphene oxide nanoparticles were incorporated to enhance the mechanical properties of the scaffolds. The scaffolds were produced using a freeze-drying technique. Subsequently, the fabricated scaffolds were evaluated through various tests, including morphology assessment via SEM, functional group analysis using FTIR, as well as assessments of swelling, biodegradability, and mechanical and biological properties. The results obtained are presented below. The morphology of porous three-dimensional scaffolds was analyzed using optical and scanning electron microscopy, revealing plate-like layers with increased GO. FTIR spectroscopy identified functional groups in graphene oxide, albumin, and gelatin. Increased GO enhanced oxygen and carbon content, while drug release studies showed better control with the G.5%Al.3%Go scaffold. Swelling tests indicated reduced swelling with higher GO, and biodegradation assessments revealed a 35% degradation for G.10%Al.3%Go. Mechanical properties improved from 2 MPa to 6 MPa with GO. Biocompatibility tests showed 103% cell viability for G.10%Al.3%Go, and antibacterial tests indicated effective inhibition.

Suggestions

Animal studies will focus on the optimal scaffolds, investigating in vivo tests to evaluate the tissue response and behavior of living organisms in comparison to the optimal sample. This research aims to assess how the scaffolds perform in a biological environment, providing insights into their effectiveness and biocompatibility for potential therapeutic applications.

Acknowledgment

We would like to express our gratitude to the Department of Biomedical Engineering at Islamic Azad University, Tehran, Iran, for providing the resources and support necessary for this research. We also appreciate the contributions of our colleagues and collaborators who have provided valuable insights throughout the study.

Authors contributions
All authors contributed equally to the conception, design, execution, and writing of this work. All authors read and approved the final manuscript.

Availability of data and materials
The datasets generated during and/or analyzed during the current study are available from the corresponding author on reasonable request.

Conflict of interests
The authors declare that they have no known competing financial interests or personal relationships that could have appeared to influence the work reported in this paper.

References

Abdelhamid H. N., Hussein K. H. (2021) Graphene oxide as a carrier for drug delivery of methotrexate. *Biointerface Res. Appl. Chem* 11:14726–14735.

Alili-Firoozinezhad S., Rajabi-Zeleti S., Mohammadi P., Gaudiello E., Bonakdar S., Solati-Hashjin M., Marsano A., Aghdami N., Scherberich A., Baharvand H. (2015) Facile fabrication of egg white macroporous sponges for tissue regeneration. *Advanced Healthcare Materials* 4 (15): 2281–2290.

Alimirzaei S., Barbaz-Isfahani R., Khodaei A., Najafabadi M. A., Sadighi M. (2024) Investigating the flexural behavior of nanomodified multi-delaminated composites using acoustic emission technique. *Ultrasonics* 138:107249.

Alizadeh M., Abbasi F., Khoshfetrat A. B., Ghaleh H. (2013) Microstructure and characteristic properties of gelatin/chitosan scaffold prepared by a combined freeze-drying/leaching method. . *Materials Science and Engineering: C* 33 (7): 3958–3967.

Andrijanto E., Shoelarta S., Subiyanto G., Rifki S. (2016) Facile synthesis of graphene from graphite using ascorbic acid as reducing agent. *AIP Conference Proceedings* 1725 (1)

Asefnejad A. (2024) Development of a Sodium Alginate/Chitosan Nanocomposite Scaffold Incorporating Zircon Nanoparticles-Hydroxyapatite, and Alendronic Acid for Bone Tissue Engineering. *Iran. J. Chem. Chem. Eng.(IJCCE)* 43 (3)

Attaeyan A., Shahgholi M., Khandan A. (2024) Fabrication and characterization of novel 3D porous Titanium-6Al-4V scaffold for orthopedic application using selective laser melting technique. *Iran. J. Chem. Chem. Eng.(IJCCE)* 43 (1)

Azimi E., Reddy V. B., Lerner E. A. (2017) MRGPRX2, atopic dermatitis, and red man syndrome. *Itch (Philadelphia, Pa.)* 2 (1): e5.

Bahari M., Chaharom M. E. E., Daneshpooy M., Gholizadeh S., Pashayi H. (2019) Effect of bleaching protocols on surface roughness and biofilm formation on silorane-based composite resin. *Dental Research Journal* 16 (4)

Bahari M., Oskoee S. S., Chaharom M. E. E., Kahnamoui M. A., Gholizadeh S., Davoodi F. (2021) Effect of accelerated aging and double application on the dentin bond strength of universal adhesive system. *Dental Research Journal* 18 (1): 25.

Barbaz-Isfahani R., Dadras H., Saber-Samandari S., Taherzadeh-Fard A., Liaghat G. (2023a) A comprehensive investigation of the low-velocity impact response of enhanced GFRP composites with single and hybrid loading of various types of nanoparticles. *Heliyon* 9 (5)

Barbaz-Isfahani R., Dadras H., Taherzadeh-Fard A., Zarezadeh-Mehrizi M. A., Saber-Samandari S., Salehi M., Liaghat G. (2022) Synergistic effects of incorporating various types of nanoparticles on tensile, flexural, and quasi-static behaviors of GFRP composites. *Fibers and Polymers* 23 (7): 2003–2016.

Barbaz-Isfahani R., Khalvandi A., Tran T. M. N., Kamarian S., Saber-Samandari S., Song J. I. (2023b) Synergistic effects of egg shell powder and halloysite clay nanotubes on the thermal and mechanical properties of abacá/polypropylene composites. *Industrial Crops and Products* 205:117498.

Barbaz-Isfahani R., Saber-Samandari S., Salehi M. (2023c) Experimental and numerical research on healing performance of reinforced microcapsule-based self-healing polymers using nanoparticles. *Journal of Reinforced Plastics and Composites* 42 (3-4): 95–109.

Berke R., Singh A., Guralnick M. (2012) Atopic dermatitis: An overview. *American Family Physician* 86 (1): 35–42.

Carr W. W. (2013) Topical calcineurin inhibitors for atopic dermatitis: review and treatment recommendations. *Pediatric Drugs* 15 (4): 303–310.

Dadras H., Teimouri A., Barbaz-Isfahani R., Saber-Samandari S. (2023) Indentation, finite element modeling and artificial neural network studies on mechanical behavior of GFRP composites in an acidic environment. *Journal of Materials Research and Technology* 24:5042–5058.

Dehkordi N. K., Shojaei S., Asefnejad A., Hassani K., Benisi S. Z. (2023) The effect of three types of cross-linked hydrogels and volume fraction of polyacrylamide on the swelling and thermal behavior using molecular dynamics simulation. *Journal of Materials Research and Technology* 24:4627–4638.

Derkach S. R., Kuchina Y. A., Baryshnikov A. V., Kolotova D. S., Voron'ko N. G. (2019) Tailoring cod gelatin structure and physical properties with acid and alkaline extraction. *Polymers* 11 (10): 1724.

Dong X., Zhang Y. Q. (2020) An insight on egg white: From most common functional food to biomaterial application. *Journal of Biomedical Materials Research Part B: Applied Biomaterials*

Farazin A., Torkpour Z., Dehghani S., Mohammadi R., Fahmy M. D., Saber S. S., Khandan A. (2021) A review on polymeric wound dress for the treatment of burns and diabetic wounds.

Farrar G., Barone J, Morgan A. (2010) Ovalbumin-BasedPorous Scaffolds for Bone Tissue Regeneration. *Journal of Tissue Engineering* 1 (1): 209860.

Ghafari Y., Asefnejad A., Ogbemudia D. O. (2024) Gold nanoparticles in biomedicine: advancements in cancer therapy, drug delivery, diagnostics, and tissue regeneration. *Scientific Hypotheses* 1:21–35.

Ghomi F., Asefnejad A., Daliri Joupari M., Goodarzi V., Hemati M. (2024) An Innovative Approach: Soft Plasma-Modified Polycaprolactone-Alginate Nanofiber Bioactive Glass with Silver Nanoparticles and PRP for Bone Tissue Regeneration. *Iran. J. Chem. Chem. Eng.(IJCCE)* 43 (3)

Gitiara Y., Barbaz-Isfahani R., Saber-Samandari S., Sadighi M. (2021) Low-velocity impact behavior of incorporated GFRP composites with nanoclay and nanosilica in a corrosive environment: experimental and numerical study. *Journal of Composite Materials* 55 (27): 3989–4010.

Grajales D. B., Sewdat N., Leo R., Kar S. (2023) Unveiling Abrocitinib: A Thorough Examination of the 2022 USFDA-Approved Treatment for Atopic Dermatitis (AD). *Medicine in Drug Discovery,* 100161.

Guo L., Niu X., Chen X., Lu F., Gao J., Chang Q. (2022) 3D direct writing egg white hydrogel promotes diabetic chronic wound healing via self-relied bioactive property. *Biomaterials* 282:121406.

Homem N. C., Miranda C. S., Teixeira M. A., Teixeira M. O., Domingues J. M., Seibert D., Antunes J. C., Amorim M. T. P., Felgueiras H. P. (2022) Graphene oxide-based platforms for wound dressings and drug delivery systems: A 10 year overview. *Journal of Drug Delivery Science and Technology* 78:103992.

Hoseini-Ghahfarokhi M., Mirkiani S., Mozaffari N., Abdolahi Sadatlu M. A., Ghasemi A., Abbaspour S., Akbarian M., Farjadian F., Karimi M. (2020) Applications of graphene and graphene oxide in smart drug/gene delivery: is the world still flat? *International Journal of Nanomedicine,* 9469–9496.

Hu K. W., Liu T. M., Chung K. Y., Huang K. S., Hsieh C. T., Sun C. K., Yeh C. S. (2009) Efficient near-IR hyperthermia and intense nonlinear optical imaging contrast on the gold nanorod-in-shell nanostructures. *Journal of the American Chemical Society* 131 (40): 14186–14187.

Hu Y., Yu B., Jia Y., Lei M., Li Z., Liu H., Huang H., Xu F., Li J., Wei Z. (2023) Hyaluronate-and gelatin-based hydrogels encapsulating doxycycline as a wound dressing for burn injury therapy. *Acta Biomaterialia* 164:151–158.

Huang Y., Zeng M., Ren J., Wang J., Fan L., Xu Q. (2012) Preparation and swelling properties of graphene oxide/poly (acrylic acid-co-acrylamide) super-absorbent hydrogel nanocomposites. *Colloids and Surfaces A: Physicochemical and Engineering Aspects* 401:97–106.

Jaberi N., Fakhri V., Zeraatkar A., Jafari A., Uzun L., Shojaei S. (2022) Preparation and characterization of a new bio nanocomposites based poly(glycerol sebacic-urethane) containing nano-clay (Cloisite Na+) and its potential application for tissue engineering. *Reactive and Functional Polymers* 170:105126.

Jasemi A., Moghadas B. K., Khandan A., Saber-Samandari S. (2022) A porous calcium-zirconia scaffolds composed of magnetic nanoparticles for bone cancer treatment: Fabrication, characterization and FEM analysis. *Ceramics International* 48 (1): 1314–1325.

Javidan Bashiz N., Asefnejad A., Ramezani Saadatabad A. (2024) Polycaprolactone/Cellulose Acetate/Polycaprolactone Scaffolds: Investigation of Absorption, Kinetics, and Controlled Release of Anticancer Drugs. *Iranian Journal of Chemistry and Chemical Engineering* 43 (5): 1890–1904.

Kalil H., Maher S., Bose T., Bayachou M. (2018) Manganese oxide/hemin-functionalized graphene as a platform for peroxynitrite sensing. *Journal of The Electrochemical Society* 165 (12): G3133.

Kamarian S., Khalvandi A., Tran T. M. N., Barbaz-Isfahani R., Saber-Samandari S., Song J. I. (2023) Predicting ESP and HNT effects on the mechanical properties of eco-friendly composites subjected to micro-indentation test. *JAinr* 15 (4): 315–328.

Khandan A., Nassireslami E., Saber-Samandari S., Arabi N. (2020) Fabrication and characterization of porous bioceramic-magnetite biocomposite for maxillofacial fractures application. *Dental Hypotheses* 11 (3): 74–85.

Kumar A., Negi Y. S., Choudhary V., Bhardwaj N. K. (2014) Effect of modified cellulose nanocrystals on microstructural and mechanical properties of polyvinyl alcohol/ovalbumin biocomposite scaffolds. *Materials Letters* 129:61–64.

Kumar N., Das S., Bernhard C., Varma G. D. (2013) Effect of graphene oxide doping on superconducting properties of bulk MgB2. *Superconductor Science and Technology* 26:095008.

Liang H., Mirinejad M. S., Asefnejad A., Baharifar H., Li X., Saber-Samandari S., Khandan A. (2022) Fabrication of tragacanthin gum-carboxymethyl chitosan bio-nanocomposite wound dressing with silver-titanium nanoparticles using freeze-drying method. *Materials Chemistry and Physics* 279:125770.

Michailidou G., Bikiaris D. N. (2022) Novel 3D-Printed Dressings of Chitosan–Vanillin-Modified Chitosan Blends Loaded with Fluticasone Propionate for Treatment of Atopic Dermatitis. *Pharmaceutics* 14 (9): 1966.

Mirhaj M., Salehi S., Tavakoli M., Varshosaz J., Labbaf S., Abadi S. Amini Mosleh, Haghighi V. (2022) Comparison of physical, mechanical and biological effects of leucocyte-PRF and advanced-PRF on polyacrylamide nanofiber wound dressings: In vitro and in vivo evaluations. *Biomaterials Advances* 141:213082.

Moarrefzadeh A., Morovvati M. R., Angili S. N., Smaisim G. F., Khandan A., Toghraie D. (2023) Fabrication and finite element simulation of 3D printed poly L-lactic acid scaffolds coated with alginate/carbon nanotubes for bone engineering applications. . *International Journal of Biological Macromolecules* 224:1496–1508.

Moghadas B. K., Ghanbari N., Nasri P. (2024) Advancements in nanoparticle biosensors: Applications, properties, and considerations for improving performance and detection capabilities. *Scientific Hypotheses* 1:53–71.

Nasalapure A. V., Chalannavar R. K., Gani R. S., Malabadi R. B., Kasai D. R. (2017) Tissue Engineering of Skin: A Review. *Trends in Biomaterials & Artificial Organs* 31 (2)

Ng W. L., Yeong W. Y., Naing M. W. (2015) Cellular approaches to tissue-engineering of skin: A review. *Journal of Tissue Science & Engineering* 6 (2): 1.

Oudeh Kadhim A., Asefnejad A., Hassanzadeh Nemati N. (2024) Fabrication and investigation of 3D scaffold using hydroxyapatite and gelatin nanoparticles for bone cancer treatment with sufficient chemical stability. *Iranian Journal of Chemistry and Chemical Engineering* 43 (5): 1872–1889.

Piao Y., Chen B. (2016) One-pot synthesis and characterization of reduced graphene oxide–gelatin nanocomposite hydrogels. *Rsc Advances*

Qian W. M., Vahid M. H., Sun Y. L., Heidari A., Barbaz-Isfahani R., Saber-Samandari S., Toghraie D. (2020) Investigation on the effect of functionalization of single-walled carbon nanotubes on the mechanical properties of epoxy glass composites: Experimental and molecular dynamics simulation. *Journal of Materials Research and Technology* 12:1931–1945.

Rahmani F., Barbaz-Isfahani R., Saber-Samandari S., Salehi M. (2023a) Effect of corrosive environment on mechanical properties of polymer-based nanocomposite: analytical and experimental study. *Materials Today Communications* 36:106544.

——— (2023b) Experimental and analytical investigation on forced and free vibration of sandwich structures with reinforced composite faces in an acidic environment. *Heliyon* 9:10.

Raisi A., Asefnejad A., Shahali M., Doozandeh Z., Kamyab Moghadas B., Saber-Samandari S., Khandan A. (2020) A soft tissue fabricated using a freeze-drying technique with carboxymethyl chitosan and nanoparticles for promoting effects on wound healing. *Journal of Nanoanalysis* 7 (4): 262–274.

Rajaei A., Kazemian M., Khandan A. (2022) Investigation of mechanical stability of lithium disilicate ceramic reinforced with titanium nanoparticles. *Nanomedicine Research Journal* 7 (4): 350–359.

Safaei M. M., Abedinzadeh R., Khandan A., Barbaz-Isfahani R., Toghraie D. (2023) Synergistic effect of graphene nanosheets and copper oxide nanoparticles on mechanical and thermal properties of composites: Experimental and simulation investigations. *Materials Science and Engineering: B* 289:116248.

Sangeetha R., Madheswari D., Priya G. (2018) Fabrication of poly (methyl methacrylate)/Ce/Cu substituted apatite/Egg white (Ovalbumin) biocomposite owning adjustable properties: towards bone tissue rejuvenation. *Journal of Photochemistry and Photobiology B: Biology* 187:162–169.

Shahmirzadi E. K., Mahale R. S., Ogbemudia D. O. (2024) Assessing the societal value of sports engagement: evidence to support active living as intrinsic to sustainable asian urbanization. *Scientific Hypotheses* 1:4–20.

Sheikhbahei E., Ari A. A. (2024) Harnessing the power of emerging digital technologies for improved sustainability and productivity in biomedical engineering and neuroscience. *Scientific Hypotheses* 1:47–52.

Shuai C., Guo W., Wu P., Yang W., Hu S., Xia Y., Feng P. (2018) A graphene oxide-Ag co-dispersing nanosystem: Dual synergistic effects on antibacterial activities and mechanical properties of polymer scaffolds. *Chemical Engineering Journal* 347:322–333.

Tavakoli M., Mirhaj M., Labbaf S., Varshosaz J., Taymori S., Jafarpour F., Salehi S., Abadi S. Amini Mosleh, Sepyani A. (2022) Fabrication and evaluation of Cs/PVP sponge containing platelet-rich fibrin as a wound healing accelerator: An *in vitro* and *in vivo* study. *International Journal of Biological Macromolecules* 204:245–257.

Tavakoli M., Najafinezhad A., Mirhaj M., Karbasi S., Varshosaz J., Al-Musawi M. H., Madaninasab P., et al. (2024) Graphene oxide-encapsulated baghdadite nanocomposite improved physical, mechanical, and biological properties of a vancomycin-loaded PMMA bone cement. *J Biomater Sci Polym Ed.* 35 (6): 823–850.

Wang L., Liu F., Zhai X., Dong W., Wei W., Hu Z. (2023a) An adhesive gelatin-coated small intestinal submucosa composite hydrogel dressing aids wound healing. *International Journal of Biological Macromolecules* 241:124622.

Wang W., Lin S., Ye Z., Zhou Y., Zou Q., Zheng T., Ding M. (2023b) Electrospun egg white protein/polyvinyl alcohol/graphene oxide fibrous wound dressing: Fabrication, antibacterial, cytocompatibility and wound healing assay. *Colloids and Surfaces A: Physicochemical and Engineering Aspects* 658:130658.

Wang Y., Zhai W., Zhang H., Cheng S., Li J. (2023c) Injectable Polyzwitterionic Lubricant for Complete Prevention of Cardiac Adhesion. *Macromolecular Bioscience,* 2200554.

Yang K., Wan J., Zhang S., Tian B., Zhang Y., Liu Z. (2012) The influence of surface chemistry and size of nanoscale graphene oxide on photothermal therapy of cancer using ultra-low laser power. *Biomaterials* 33 (7): 2206–2214.

Zakavi F., Gholizadeh S., Dibazar S., Esmaeili M. (2023) A comparison of laser and mechanical surface pretreatment methods on shear bond strength of resin composite to resin-modified glass ionomer. *Journal of Dentistry* 24 (1): 103.

Zhao Q., Chen D., Li Y., Zhang G., Zhang F., Fan X. (2012) Rhodium Metal Complex Immobilized on Graphene Oxide as Efficient and Recyclable Catalyst for Hydrogenation of Cyclohexene.

Zhou Y., Li L., Yu Z., Gu X., Pan R., Li Q., Cui Y. (2022) Dermatophagoides pteronyssinus allergen Der p 22: Cloning, expression, IgE-binding in asthmatic children, and immunogenicity. *Pediatric Allergy and Immunology* 33 (8): e13835.